Forest Ecology and Management 520 (2022) 120392

Contents lists available at ScienceDirect

Forest Ecology and Management

journal homepage: www.elsevier.com/locate/foreco

Integration of carbon dioxide concentration in a simplified process-based model for evapotranspiration estimation in an old-growth forest

Meiting Liu [a,b,c], Hailong Wang [a,b,c,*], Xiaodong Liu [d,*], Bingjun Liu [a,b,c], Xiaohong Chen [a,b,c], Qianmei Zhang [e], Ze Meng [e]

[a] School of Civil Engineering, Sun Yat-sen University, Guangzhou 510275, China
[b] Southern Marine Science and Engineering Guangdong Laboratory, Zhuhai, Guangdong 519082, China
[c] Guangdong Engineering Technology Research Center of Water Security Regulation and Control for Southern China, Sun Yat-sen University, Guangzhou 510275, China
[d] College of Forestry and Landscape Architecture, South China Agricultural University, Guangzhou 510642, China
[e] South China Botanical Garden, Chinese Academy of Sciences, Guangzhou 510650, China

ARTICLE INFO

Keywords:
Climate change
Evapotranspiration
Carbon dioxide concentration
Water use efficiency
Water-carbon coupling
Subtropical forest

ABSTRACT

Evapotranspiration (ET) is one of the most difficult hydrologic variables to estimate. In the context of climate change, the rise of CO_2 emissions may improve photosynthesis but depress transpiration thus increasing plant water use efficiency (WUE). Therefore, it is of great importance and necessity to take elevated atmospheric CO_2 concentration (Ca) as a limiting factor for improved assessment of ET and WUE toward a better ecosystem management. In this study, we developed and incorporated a Ca stress function into a modified process-based transpiration model and extended its application from transpiration to total evapotranspiration simulation. The original simplified process-based model (denoted as BTA by combining developers' last name initials), previously modified version with added soil moisture (BTA-θ) and the extended version in this study with CO_2 concentration (BTA-Ca) were tested for daily ET simulation at the Dinghushan forest ecosystem in south China. The results show that eddy covariance based forest ET was well simulated by the models, while the two modified models outperformed the original one. Despite the limited improvement of accuracy, the BTA-Ca model is more superior and meaningful regarding the physical mechanisms. Moreover, we evaluated the biophysical responses of ET and GPP to the major environmental factors, which shows that ET and GPP responded similarly to environmental changes with close linkages between the two. This study proposed a Ca stress function and provides an effective way of coupling water and carbon exchange processes for ET simulations, which can be applied for forest water budget assessment under climate change.

1. Introduction

Evapotranspiration (ET) is an integrated term representing soil evaporation and vegetation transpiration. Globally, annual ET returns over 60% of precipitation to the atmosphere (Oki and Kanae, 2006) which makes it the second largest component of the terrestrial water cycle (Pascolini-Campbell et al., 2021), and it is expected to intensify under future climate with rising temperature induced by increasing atmospheric CO_2 concentration (Greve et al., 2014; Held and Soden, 2006; Huntington, 2006). As an important hydrologic variable, ET is closely coupled with the carbon cycle and energy balance (Anderson et al., 2008; Fisher et al., 2017; Kothavala et al., 2005; Wang, 2007; Xiang et al., 2020) through leaf stomates behavior (Sitch et al., 2008; Xu et al., 2018). Although the basic physics of ET is well understood, we still have some difficulties in estimating ET accurately (Wang et al., 2017; Wang and Bras, 2011).

At present, many methods have been developed to quantify ET. Field techniques like precision weighing lysimeter, Bowen ratio and eddy covariance techniques can quantify ET from a homogeneous surface area with continuous labor and capital inputs (Allen et al., 2011; Baldocchi et al., 2001; Scott et al., 2000). Remote sensing algorithms provide an alternative way of ET estimation to overcome the spatiotemporal scale issues existing in field techniques, however, its application is usually limited by spatial and temporal resolution of satellite imagery and cloudy sky conditions (Shwetha and Nagesh, Kumar, 2015). Models can help understand well the water flow and storage in a catchment area, but

* Corresponding authors at: School of Civil Engineering, Sun Yat-sen University, Guangzhou 510275, China (H. Wang).
E-mail addresses: wanghlong3@mail.sysu.edu.cn (H. Wang), liuxd@scau.edu.cn (X. Liu).

https://doi.org/10.1016/j.foreco.2022.120392
Received 14 February 2022; Received in revised form 22 June 2022; Accepted 24 June 2022
Available online 30 June 2022

there are still challenges in modeling and validating the results (Ala-aho et al., 2017). Among ET models some rely on air temperature (Hargreaves and Samani, 1982), or net radiation in addition to air temperature (Priestley and Taylor, 1972), and the relative simplicity makes them attractive but may lead to serious deviations in hydrological forecasts under future climatic changes (Cristea et al., 2013; Milly and Dunne, 2017; Seiller and Anctil, 2016; Xiang et al., 2020). With added complexity, the Penman-Monteith equation (Monteith, 1965) requires more meteorological inputs and surface resistance parameterization to estimate ET. Following a similar philosophy, there have been numerous studies estimating total ET or its components by linking them explicitly with a set of environmental variables, for example, the Jarvis-Stewart scheme and the Penman-Monteith-Leuning model (Garcia et al., 2013; Jarvis, 1976; Stewart, 1988; Wang et al., 2014; Zhang et al., 2019).

Process-based models have also been developed to estimate transpiration (Federer, 1979; Gao et al., 2002). These models include parameters that explicitly represent measurable biophysical properties like leaf-specific hydraulic conductance and soil water potential, etc. Among them, Buckley, Mott and Farquhar (2003) proposed a model to calculate canopy conductance based on hydromechanical and biochemical process laws with also explicit consideration of the mechanical advantage of the epidermis. In their model, three different biophysical effects - the guard cell metabolic advantage ($\beta\tau$), the epidermal mechanical advantage (M), and the guard cell resistive advantage (ρ), were incorporated into a single parameter to be estimated empirically, i.e., $\alpha = \beta\tau – M + \rho$. The biochemical substructure of the model which controls the response to atmospheric CO_2 concentration (hereafter Ca), irradiance, and oxygen was embedded in τ (ATP concentration) or α (the guard cell advantage). Therefore, the model indirectly reflects the response to those environmental factors via their effects on photosynthesis. This model is good for understanding the biophysical and biochemical processes within the plant, but difficult to apply for an extended spatial scale for conductance or water use simulations due to limited availability of the required model inputs. To overcome this issue, Buckley, Turnbull, and Adams (2012) simplified the model for whole tree sap flow and transpiration modeling with significantly reduced inputs, which was later cited as the "BTA" model by Wang et al., (2016) using their last name initials. The BTA model is easy to apply because it only requires solar radiation and vapor pressure deficit measurements with only 3 parameters for daily and 4 parameters for sub-daily simulations, and it can capture wide biological variations and effects of climate change. However, the model has some limitations as Wang et al., (2016) pointed out that the model performance may be restricted because it only considers the controls of atmospheric variables on plant water use but not the soil water content. Later on, a modified version of this model was tested with an added soil water potential (ψ) function (Liu et al., 2019a), and then a soil water content (θ) function for the convenience of measurement and application (Liu et al., 2019b).

In addition to the hydrometeorological variables such as temperature, wind speed, precipitation and solar radiation, ET is also modulated by changes in environmental factors like the atmospheric CO_2 concentration (Ca), nitrogen and aerosol deposition (Piao et al., 2015; Shi et al., 2013). The atmospheric CO_2 concentration can exert strong impacts on ET mainly in two ways. On the one hand, elevated Ca may reduce transpiration by decreasing leaf stomatal conductance after intercellular Ca saturation for photosynthesis (Bernacchi et al., 2007; Xie et al., 2020); on the other hand, Ca can stimulate plant growth via the effect of fertilization, resulting in an increase of the leaf area and vegetation coverage to increase ET (Piao et al., 2015; Shi et al., 2013). Whether the overall effect of Ca increase on ET is positive or negative will depend on which of the above-mentioned process dominates (Hussain et al., 2013; Kruijt et al., 2008; Liao et al., 2021; Liu et al., 2021; Lovelli et al., 2010). A recent study has shown that canopy transpiration declines at about 5.1% per 100 ppmv (parts per million, by volume) increase in Ca level (Gopalakrishnan et al., 2011). Because of the tight relationships between the Ca and ET, it is necessary and important to incorporate Ca into ET models toward accurate estimation of ET under future climate change and improved understanding of the coupling between water and carbon cycles (Fisher et al., 2017).

In this study, we hypothesize that the BTA model will be improved regarding ET estimation with Ca effect considered. We formulated a Ca stress function and incorporated it into the previously modified BTA-θ model, and the final version was named BTA-Ca. We then used the models in a subtropical old-growth forest ecosystem, aiming to extend the capability of the model for total evapotranspiration simulation. Therefore, the specific objectives were: (1) to analyze the responses of evapotranspiration, gross primary production to primary environmental factors at a humid subtropical dense forest site; and (2) to evaluate the modified models regarding the effect of soil moisture and carbon dioxide concentration on the total evapotranspiration estimation. The results of this study will help improve our understanding of water-carbon coupling processes and have implications for ecohydrological responses to future climate change.

2. Materials and methods

2.1. Site descriptions

This study used the data collected at the Dinghushan forest research station (DHS) located ~ 90 km west to Guangzhou City (112°30′39″-112°33′41″E, 23°09′21″–23°11′30″N), which was the first National Natural Reserve in China in 1956 (Fig. 1). With a south subtropical monsoon climate, the study site has an average annual temperature of 20.9 °C and an average annual precipitation of 1678 mm of which more than 80% is concentrated in the wet season (April-September). DHS has a total area of 1156 ha and the main terrains are hills and low mountains with the altitude ranging from 100 to 700 m mostly, and the highest peak, Keelung Mountain, has an altitude of 1000.3 m (Liu et al., 2015).

The soil type is mainly characterized as lateritic red soil developed from sandstone and sand shale, distributed below 400–500 m altitude. The forest in the reserve is mature with trees over 100 years old and a few young forests have also been established in recent decades. In the past 60 years, the reserve has been relatively intact and has not been disturbed. The dominant vegetation at the study site is southern subtropical evergreen broad-leaved forest with an average tree height of 19.5 m and transitional vegetation types are Monsoon evergreen broad-leaved forest (MBF), *Pinus massonniana* forest (PF) and Mixed *Pinus massonniana*/broad-leaved forest (PBF), which provide a natural ideal research base for the study of the succession process and pattern of the forest ecosystem (Liu et al., 2013; Zhou et al., 2005).

2.2. Meteorological data and evapotranspiration

Eddy covariance (EC) measurements of turbulent fluxes of sensible and latent heat (H, LE), surface energy components (R_n and G) and carbon dioxide concentration (CO_2) were collected from 2007 to 2010 in the forest stand with a fetch of greater than 5 km in every direction. The sensors, including a CO_2/H_2O analyzer (Model LI-7500, Li-Cor Inc., USA) and a three-dimensional ultrasonic anemometer (CSAT3, Campbell Scientific Inc., USA), were mounted at the height of 27 m above ground on a supporting tower of 38 m tall in total, which was installed at an elevation of 80 m.a.s.l. The surrounding vegetation species include *Castanopsis chinensis*, *Canarium tramdenum*, *Schima superba*, *Cryptocarya chinensis*, *Cryptocarya concinna*, *Machilus chinensis*. The height of the forest canopy around the tower is approximately 22 m high, and the mean leaf area index (LAI) is 4.9 during the dry season and 5.6 during the wet season (Liu et al., 2017). The measurements were taken at 10 Hz, averaged over 30-min intervals, and directly recorded using the synchronous device for measurement (SDM) technique with a data logger (CR5000, Campbell Scientific Inc.) (Liu et al., 2014; Yan et al., 2013). In order to ensure the validity and quality of the flux data, the original data were corrected by quadratic coordinate transformation and ultrasonic

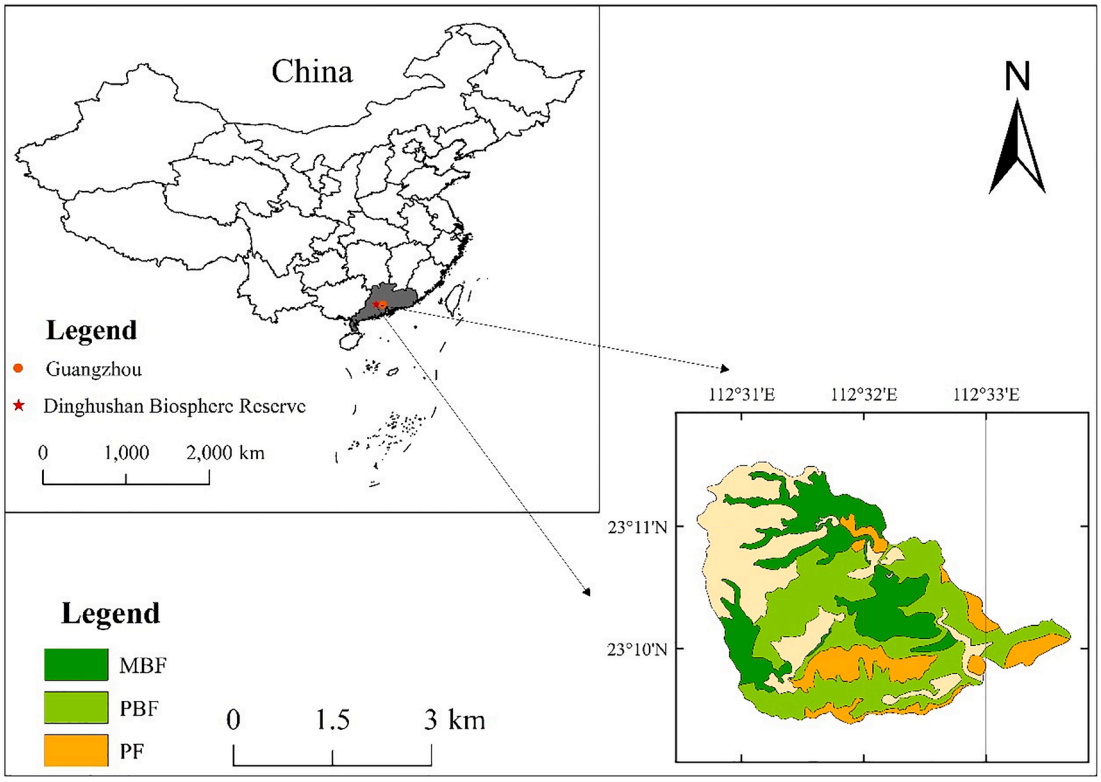

Fig. 1. Location of the Dinghushan Forest Ecosystem Research Station in south China. MBF: Monsoon evergreen broad-leaved forest; PBF: Mixed *Pinus massonniana*/ broad-leaved forest; PF: *Pinus massonniana* forest.

temperature correction, and the influence of topography and instrument tilt was also corrected. The air density fluctuation correction and interpolation was modified for Webb-Pearman and Leuning (WPL) density corrections (Webb et al., 1980). Evapotranspiration was calculated based on the latent heat flux (*LE*) measurement using Eq. (1).

$$ET = \frac{LE}{\lambda} \tag{1}$$

where λ is latent heat of vaporization (MJ/kg) and *LE* is latent heat flux (MJ/m^2/day). We are aware that due to many potential reasons (Mallick et al., 2016; Twine et al., 2000; Xu et al., 2019), the latent heat flux obtained from eddy covariance measurements is often affected by an imbalance problem in the energy budget, i.e. $LE + H < R_n - G$ (Maruyama et al., 2019). Here, *LE* data was obtained after processing by Li et al., (2020b).

Along with the above flux measurements, standard meteorological data were collected at 0.5 Hz, including temperature, humidity, solar radiation, wind speed, soil moisture and precipitation, by a micrometeorological observation system (Milos 520, Vaisala) at a height of 27 m on the same tower with the EC flux measurements. All of the routine meteorological data were recorded at 30-min intervals (Yan et al., 2013; Zhou et al., 2005). Vapor pressure deficit (*D*, kPa) was calculated based on the measured air temperature, humidity and actual water vapor pressure above the forest canopy. Gross primary productivity (GPP, g C/m^2) was calculated as the sum of measured net ecosystem carbon exchange and ecosystem respiration.

2.3. Descriptions of model development

2.3.1. The simplified process-based model

The process-based model used in this study was initially proposed to estimate canopy conductance (Buckley et al., 2003), which was then simplified for stand transpiration and canopy conductance (Buckley et al., 2012). The simplified model was later denoted as the "BTA" model given in Eq. (2) for sub-daily transpiration simulations:

$$E_t = E_{\max} \cdot \frac{(R_s + R_0)D}{k + bR_s + (R_s + R_0)D} \tag{2}$$

where E_t is the transpiration rate (mm/d), $E_{\max}$ is the maximum transpiration rate which in many previous studies was considered as a fitted parameter (mm/d) or the maximum value of the measured transpiration (Liu et al., 2019b, 2019a; Xu et al., 2017). Parameters k (kPa W/m^2) and b (kPa) are fitted with site specific observation data. R_s (W/m^2) is measured solar radiation and D (kPa) is the leaf to air vapor pressure deficit in its original version, which was replaced with air vapor pressure deficit in this study (using the same symbol D). R_0 (W/m^2) is included in Eq. (2) to enable the model to simulate nocturnal transpiration/sap flow, and is set as zero when used to simulate daily total transpiration (Buckley et al., 2012; Liu et al., 2019b, 2019a).

2.3.2. The modification of BTA model with soil water constraint

The BTA model was modified by Liu et al., (2019a) initially with a linear stress function of soil water potential, ranging from 0 to 1, and later with different forms of soil water content (θ) functions (Liu et al., 2019b) to account for soil water limitation besides the atmospheric conditions for transpiration estimation. This version is denoted as the BTA-θ here and given in Eq. (3).

$$E_t = E_{\max} \cdot \frac{R_s D}{k + bR_s + R_s D} f(\theta) \tag{3}$$

where $f(\theta)$ represents the stress function of volumetric soil water content. $f(\theta) = 1$ means that the soil is saturated with water and not limiting transpiration, while $f(\theta) = 0$ means that the soil is extremely dry and the transpiration process ceases.

Soil water content is a main limiting factor in evapotranspiration and its components especially in drylands, because soil water content is the water source for evapotranspiration. Limitation of soil water content on evapotranspiration is complex and often nonlinear (Alkama and

Cescatti, 2016). Different types of soil water content stress functions may lead to different model performance (Wang et al., 2016; Xu et al., 2018). Therefore, to better show the performance of the model and accurately predict evapotranspiration in a subtropical forest, we reviewed existing studies regarding transpiration modeling with environmental variables and found three widely applied forms of $f(\theta)$. The first was originated in Jarvis (1976) and used in Liu et al., (2019b):

$$f_1(\theta) = 1 - e^{-k_1(\theta-\theta_1)} \tag{4}$$

where k_1 is a fitted parameter. When k_1 (-) increases, $f_1(\theta)$ decreases; parameter θ_1 is the value of soil water content at which the relation extrapolates to $f_1(\theta) = 0$. The second one is given in Eq. (5), often found in the literature for evapotranspiration estimates (Busscher, 1980) and also discussed in Liu et al., (2019b):

$$f_2(\theta) = \min\left(1,\ \frac{\theta - \theta_w}{\theta_c - \theta_w}\right) \tag{5}$$

where θ_w and θ_c represent permanent wilting point moisture content (cm^3cm^{-3}) and field capacity (cm^3cm^{-3}), respectively, which were taken as parameters in this study. When the soil water content is between θ_w and θ_c, a linear relationship is presumed between evapotranspiration and soil water content. A third soil water stress function (Eq. (6)) takes the sigmoidal instead of linear relationship which results in relatively better performance in terms of fitting low-end of soil water content (Guyot et al., 2017; Whitley et al., 2013).

$$f_3(\theta) = \frac{1 + e^{-k_2\theta}}{1 + e^{-k_2(\theta-k_3)}} \tag{6}$$

where k_2 is a parameter describing a change of evapotranspiration with a decrease of soil water content, and k_3 is the parameter of soil water content wilting point at a specific site.

2.3.3. The further modifications of BTA-θ model with carbon dioxide concentration

This study made two further modifications to the modified model in Eq. (3). Firstly, the model was extended to simulate daily total evapotranspiration rather than just transpiration or sap flow by modifying Eq. (3) to the form in Eq. (7). This is feasible because we measured the T_a, R_s, etc. above the forest canopy, which eventually reflects the effect of energy and water exchange between the entire forest (including understory plants) and the air above. Note that the prescribed E_{max} in Eq. (3) following previous method (i.e. maximum measured value) may limit the ability of the model to adjust its performance to correctly reflect the effect of soil water availability, and often leads to underestimation of the target flux (Wang et al., 2020, 2016; Xu et al., 2017). On the other hand, potential evapotranspiration can reflect seasonal meteorological variations and is generally greater than actual evapotranspiration. Therefore, reference evapotranspiration (ET_o) calculated by the FAO-56 Penman-Monteith Eq. (8) was used to replace a fitted or prescribed E_{max} in our study.

$$ET = ET_0 \cdot \frac{R_s D}{k + bR_s + R_s D} f(\theta) \tag{7}$$

$$ET_0 = \frac{0.408\Delta(R_n - G) + \gamma\dfrac{900}{T_a + 273}u_2 D}{\Delta + \gamma(1 + 0.34u_2)} \tag{8}$$

where R_n is net radiation (MJ/m^2/day), G is soil heat flux (MJ/m^2/day), Δ is the slope of the vapor pressure curve (kPa/°C), T_a is air temperature (°C), D is air vapor pressure deficit (kPa), γ is psychrometric constant (kPa/°C) and u_2 is wind speed at 2 m height (m/s).

A further modification we made to the model in Eq. (7) was to integrate a stress function of the atmospheric CO_2 concentration (Ca). The final derived model is denoted as BTA-Ca hereafter, given in Eq. (9).

$$ET = ET_o \cdot \frac{R_s D}{k + bR_s + R_s D} f(\theta) f(C_a) \tag{9}$$

where f(Ca) is a response function of Ca ranging from 0 to 1. A value of 1 indicates the best carbon sequestration condition while a value of 0 expresses extreme carbon starvation. The advantage of the BTA-Ca model lies in the integration of f(Ca) which allows the model to explore the effects of global climate change on the terrestrial hydrologic cycle. This has not been seen in other empirical or mechanistic ET models related to environmental variables.

Going through the literature, we found that a Ca stress function for ET simulation is rarely developed and discussed, here we constructed a sigmoidal function based on the scatter plot of ET-Ca data, given in Eq. (10).

$$f(C_a) = e^{\frac{-k_4(C_a - k_5)^2}{C_a + k_5}} \tag{10}$$

where k_4 and k_5 are considered as fitting parameters that determine the shape of the response curve. Such a S-shape curve is able to cover a wide range of ET and Ca values especially at the low end.

Because these environmental stress functions often perform differently at different sites, we chose all three soil water stress functions mentioned above to determine the most appropriate one applicable at our site. The modified BTA models with equations (4–6) are denoted as BTA-θ1, BTA-θ2 and BTA-θ3, respectively, and accordingly the three further modified BTA-θ models with f(Ca) are named BTA-Ca1, BTA-Ca2 and BTA-Ca3.

2.4. Bias correlation analysis

The evapotranspiration process is affected by ecological and environmental factors, the change of one element may cause changes in other elements, and the bias correlation analysis can be used to study the interrelationship between two specific variables. Bias correlation analysis refers to the process of excluding the influence of the third variable when two variables are related to the third variable at the same time, and only analyzes the correlation between the other two variables (Ye et al., 2018).

Based on the meteorological data during 2007–2010, we analyzed the bias correlation between evapotranspiration and vapor pressure deficit, solar radiation, carbon dioxide concentration and soil water content, by firstly calculating the coefficient of simple correlation and then obtaining the coefficient of bias correlation. The correlation coefficient between evapotranspiration and the above meteorological variables is calculated as:

$$R_{xy} = \frac{\sum_{i=1}^{n}[(x_i - \bar{x})(y_i - \bar{y})]}{\sqrt{\sum_{i=1}^{n}(x_i - \bar{x})^2}\sqrt{\sum_{i=1}^{n}(y_i - \bar{y})^2}} \tag{11}$$

where R_{xy} is the correlation coefficient of the two variables x and y; x_i and y_i are the values of the x and y variables, respectively; $\bar{x}$ and $\bar{y}$ are the means of the two impact factors, respectively, and i is the number of samples.

The bias correlation coefficient is calculated as:

$$R_{xy,z} = \frac{R_{xy} - R_{xz}R_{yz}}{\sqrt{1 - R_{xz}^2}\sqrt{1 - R_{yz}^2}} \tag{12}$$

where $R_{xy,z}$ is the coefficient of bias correlation between x and y after z is fixed, and R_{xy}, R_{yz}, and R_{xz} represent the correlation coefficients of x and y, y and z, and x and z, respectively. All statistical analysis was conducted in the software SPSS 26.

2.5. Model calibration and validation

In the process of data collation and analysis, the missing data caused

by instrument failure were removed, and only data for different variables that cover the same period (i.e., concurrently available) were left for further analysis. The filtered data were then randomly divided into two groups for calibration and validation of the models, respectively. The results were displayed by a tag of "Calibration" or "Validation" accordingly.

We applied the DiffeRential Evolution Adaptive Model (DREAM) to optimize the values of all the parameters in each model. The DREAM algorithm is a global optimization solution based on an advanced Markov chain Monte Carlo sampling method using multiple chains to update results at the same time. It has high computational efficiency and has been widely used for parameter optimization of models (Liu et al., 2019b; Vrugt, 2016; Wang et al., 2016).

To evaluate the model performance regarding ET simulation, we used five metrics including the linear regression slope (s), the linear regression coefficient of determination (R^2), average absolute percentage error (MAPE), root mean square error (RMSE), and Bayesian information criterion between the measured and simulated ET. Furthermore, the Bayesian information criterion (BIC) (Schwarz, 1978) penalizes inclusion of extra parameters in a model (Hawkins, 2004; Liu et al., 2019a) to test the overfitting problem. BIC is calculated as:

$$\mathrm{BIC} = n\log\left(\frac{\mathrm{SSE}}{n}\right) + m\log(n) \tag{13}$$

where n is the number of data points, SSE is the sum of squared errors, and m is the number of predictors. A model is preferred if its BIC is smaller than others (Guan et al., 2013).

3. Result

3.1. Dynamics of hydrometeorological variables

Fig. 2 shows the daily dynamics of environmental variables at the study site from 2007 to 2010, which demonstrates a high synchrony between water and energy availability as well as carbon assimilation (Fig. 2a-d). On average, the daily solar radiation was 138.6 ± 78.2 W/m^2 and the relative humidity was 76.1 ± 16.3%. There were 124 days in total during the 4 years when relative humidity exceeds 95%. The highest relative humidity existed in April and the lowest in November. The daily average temperature was 20.3 ± 6.2 °C, and the average temperatures in the coldest month (January) and the hottest month (July) were 11.2 ± 6.3 °C and 26.7 ± 6.2 °C, respectively. The average CO_2 concentration was 443.6 ± 135.2 cm^3/m^3. The average water vapor pressure deficit was 0.6 ± 0.4 kPa, and its dynamic change was highly consistent with the air temperature, reflecting the high dependence between the two variables.

The soils at the forest site had relatively high water saturation status with the mean depth-average volumetric soil water content of 0.24 ± 0.04 m^3/m^3. The change of soil water content synchronized well with precipitation, which showed high values in summer and low values in winter. The annual average precipitation was 1457 ± 387 mm with more than 83% occurred in April to September. ET and ET_o showed strong seasonal characteristics like the other variables. The annual average ET was 655.9 ± 44.3 mm, accounting for approximately 45% of the average annual precipitation. The actual ET was consistently lower than ET_o, although the difference was smaller in winter and spring than that in summer and autumn; and the annual average GPP was 1430 ± 87 g C/m^2.

It should be noted that the above calculated annual values should be lower than the true annual values because of the missing data during the

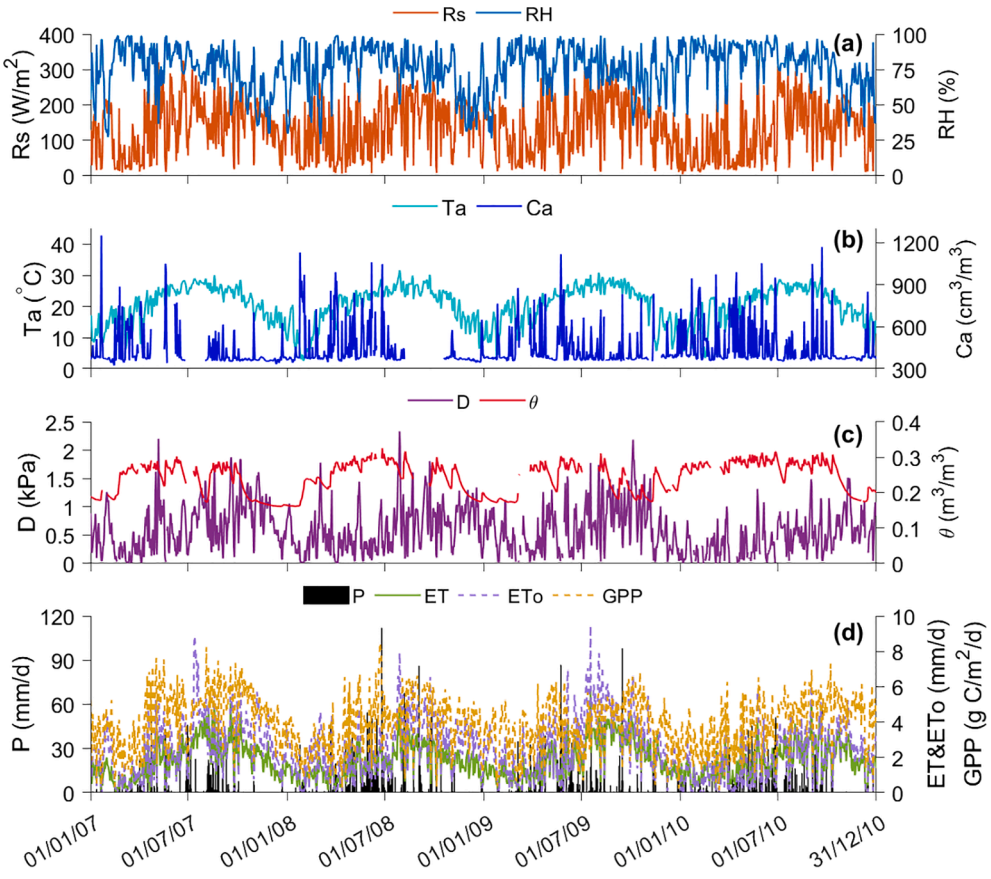

Fig. 2. Daily dynamics of hydroclimate variables at the Dinghushan Forest Station from 2007 to 2010. (a) Solar radiation (R_s) and relative humidity (RH); (b) Air temperature (Ta) and the atmospheric CO_2 concentration (Ca); (c) Water vapor pressure deficit (D) and mean soil water content from 15 cm, 30 cm, and 45 cm depths (θ); and (d) Precipitation (P), actual evapotranspiration (ET), potential evapotranspiration (ET_o) and gross primary productivity (GPP). Disconnection of the lines infers missing data.

four years due to the failure of experimental equipment and variable data availability periods. Therefore, to reduce the errors caused by the calculation of annual accumulation of precipitation, evapotranspiration, potential evapotranspiration and gross primary productivity, we gave the daily average values of these variables in each year during the entire study period for comparison (Table 1).

From 2007 to 2010, the annual average daily P in Dinghushan was 3.92 ± 10.40 mm, but it reached 5.39 ± 13.61 mm in 2008 which was considered a wet year. From Fig. 2d, we can see that 2008 had the most precipitation over the four years with 159 rainy days, and the maximum precipitation reached 111.8 mm/d. On average, the daily ET was 1.83 ± 0.98 mm accounting for about 47% of the daily P which is close to the annual cumulative value (45%), and the daily ET_o was 2.44 ± 1.59 mm accounting for approximately 62% of P, which meant that Dinghushan is in the humid zone. In this study, WUE is defined as the ratio of GPP to ET, so WUE depends on both GPP and ET. From Table 1, we can see that the annual average daily water use efficiency during the study period was 2.52 ± 1.14 g C/kg H_2O, and the inter-annual variation of Dinghushan WUE was relatively small.

3.2. Environmental impacts on evapotranspiration and gross primary production

In order to understand how evaporative flux and carbon assimilation respond to environmental changes towards improved parameterization and simulations, ET and GPP were plotted in Fig. 3 against four environmental factors including vapor pressure deficit, solar radiation, CO_2 concentration and soil water content, from which the suitability of the response functions listed in section 2.3 can also be evaluated. Fig. 3 shows that the response of daily ET to D and R_s can be expressed by linear relationships ($p < 0.001$) with regression coefficients of determination (R^2) of 0.46 and 0.55, respectively, which means that a significant linear correlation existed between evapotranspiration and vapor pressure deficit and solar radiation. This is common to observe for such relationships at daily scale. Fig. 3c shows that the main range of Ca was between 300 ~ 600 cm^3/m^3 at the study site, and ET was high at the low range of Ca and decreased with increasing Ca values. With a fixed E_{max} for a whole study period as in previous studies, the outer envelops of the data points can be drawn by multiplying the E_{max} by each stress function while setting others as 1 (such as Fig. 1 in Wang et al., 2020) to test the suitability of the stress function. However, this is not realistic with a varying ET_o on each day in this study. Nonetheless, in the context of ~ 98.6% of observations falling in the range of Ca greater than 350 cm^3/m^3, the increase of carbon dioxide concentration corresponded to the decrease of the forest ET. Such a relationship was also reported by Gedney et al., (2006), who attributed this effect to CO_2 physiological forcing, that is, when the environmental CO_2 concentration was high, the vegetation stomatal conductance decreased with reduced stomates openness to save water (Cao et al., 2010; Gopalakrishnan et al., 2011).

Table 1
A comparison of average daily precipitation (P), evapotranspiration (ET), potential evapotranspiration (ET_o), gross primary productivity (GPP) and water use efficiency (WUE) from 2007 to 2010 at Dinghushan.

Year	P (mm)	ET (mm)	ET_o (mm)	GPP (g C/m^2)	WUE (g C/kg H_2O)
2007	2.73 ± 7.36	1.90 ± 1.04	2.65 ± 1.62	4.31 ± 1.58	2.72 ± 1.23
2008	5.39 ± 13.61	1.68 ± 0.82	2.46 ± 1.48	3.82 ± 1.56	2.50 ± 0.90
2009	3.72 ± 10.31	1.98 ± 1.09	2.73 ± 1.75	3.76 ± 1.41	2.33 ± 1.22
2010	3.83 ± 9.11	1.75 ± 0.93	1.94 ± 1.34	3.89 ± 1.47	2.55 ± 1.15
Mean	**3.92 ± 10.40**	**1.83 ± 0.98**	**2.44 ± 1.59**	**3.94 ± 1.52**	**2.52 ± 1.14**

Moreover, the response of ET to θ was clearly nonlinear, considerably different from that to D and R_s, which means that the relationship between them cannot be judged simply from the linear correlation. The envelop of ET-θ data clouds can be described by a piecewise linear function as in Eq. (5) where ET maximized and kept constant in between two moisture thresholds near approximately 0.18 and 0.28 m^3/m^3 according to the parameter optimization. Based on the daily ET data of Dinghushan forest from 2007 to 2010, it was found that there was a significant linear correlation between GPP and ET under the condition of θ of 0.16 ~ 0.32 cm^3/m^3 ($R^2 = 0.52$, $p < 0.001$); in other words, there was a strong linear relationship between carbon assimilation and evapotranspiration. Notably, the interannual variation of GPP in Dinghushan forest was small and relatively stable (Table 1). The responses of GPP to environmental factors was consistent with that of ET, especially solar radiation ($R^2 = 0.55$), followed by vapor pressure deficit ($R^2 = 0.36$). Responses of GPP to Ca and θ were also nonlinear implying more sophisticated response mechanisms.

In addition, based on the bias correlation analysis results in Table 2, it was observed that in this environment D and R_s influenced ET stronger than Ca and θ, with a bias correlation coefficient of 0.70 and 0.74 ($p < 0.001$), respectively. Consistent with Fig. 3c, the atmospheric CO_2 concentration exerted overall negative but limited impact on ET with a bias correlation coefficient of −0.35 ($p < 0.001$).

3.3. Simulations of evapotranspiration by different models

3.3.1. Daily evapotranspiration modeling

ET was simulated by the original BTA model as well as the modified models (BTA-θ and BTA-Ca), and results were compared in Fig. 4 and Table 3. In both the calibration and validation periods, we found that the original model and the modified versions all simulated well the measured ET for the study site, and the performance of modified models were all better than the original one indicated by all statistical metrics. For example, the linear regression R^2 between measured and simulated ET by the original BTA model was 0.73 with a $RMSE = 0.60$ mm/d for both calibration and validation datasets; while the regression R^2 ranged 0.79 ~ 0.82 with $RMSE \leq 0.49$ mm/d for the BTA-θ group, whereas R^2 equals 0.82 with a $RMSE \leq 0.43$ mm/d for the BTA-Ca group. The *MAPE* for all the modified models was also significantly lower than that for the original BTA model.

In addition, combining all the statistical metrics in Table 3 we found that the BTA-Ca3 and BTA-θ3 outperformed the rest models in their groups. For the calibration, model BTA-θ3 resulted in a R^2 of 0.82, *MAPE* of 19.16%, *RMSE* of 0.42 mm/d and *BIC* of −316.90, while for the validation, the R^2, *MAPE* and *RMSE* was 0.81, 20.66%, 0.43 mm/d and −309.86, respectively. In comparison, the model BTA-Ca3 resulted in a R^2 of 0.82 with *MAPE* of 18.76%, *RMSE* of 0.41 mm/d and *BIC* of −321.55 for calibration, and R^2 of 0.82 with *MAPE* of 19.94%, *RMSE* of 0.42 mm/d and *BIC* of −318.53 for validation, respectively. Fig. 5 shows the fitting results of daily ET by the original BTA model, the modified BTA-θ3 and BTA-Ca3 model. It was observed that all models captured well the temporal dynamics of daily ET, and BTA-θ3 and BTA-Ca3 had better simulations than BTA; meanwhile, BTA-Ca3 proved to be more accurate than BTA-θ3 with similar R^2 but lower *RMSE* and *MAPE* as well as *BIC*. This indicates that adding a *f*(Ca) indeed can reflect the influence of CO_2 concentration on evapotranspiration and hence improve model performance. Moreover, ET simulated by these models was in good agreement with the observations in both wet and dry periods, and overestimation was obvious by the original simplified BTA model in wet periods.

3.3.2. Simulation capabilities of models under different Ca levels

In order to further examine whether the models with an added Ca function can effectively improve the ET simulation ability and to testify the necessity of incorporating a *f*(Ca) in the ET models, we compared the simulations from the model sets under different Ca levels which were

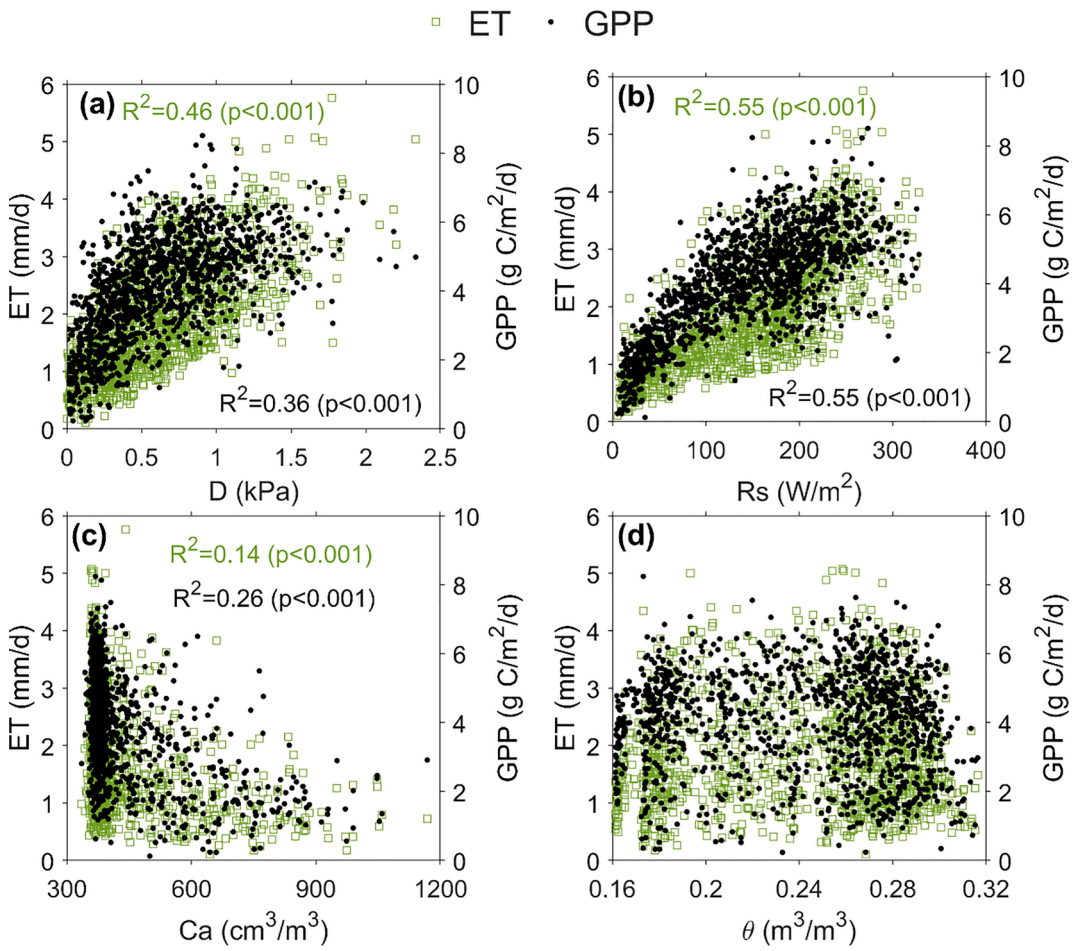

Fig. 3. Evapotranspiration (ET) and gross primary productivity (GPP) response to (a) vapor pressure deficit (D), (b) solar radiation (R_s), (c) the atmospheric CO_2 concentration (Ca), and (d) mean soil water content (θ) at depths of 15 cm, 30 cm, and 45 cm. Green square represents ET and black dot represents GPP in each plot. R^2 were obtained based on linear regressions between ET or GPP and the related environmental factors. (For interpretation of the references to colour in this figure legend, the reader is referred to the web version of this article.)

Table 2
The coefficients (R) of bias correlation analysis. *** indicates $p < 0.001$, and ** indicates $p < 0.05$.

Variables	D	R_s	Ca	θ	ET
D	1.00	0.76^{***}	-0.51^{***}	-0.30^{***}	0.70^{***}
R_s	0.76^{***}	1.00	-0.54^{***}	-0.06^{**}	0.74^{***}
Ca	-0.51^{***}	-0.54^{***}	1.00	0.27^{***}	-0.35^{***}
θ	-0.30^{***}	-0.06^{**}	0.27^{***}	1.00	0.11^{***}
ET	$\mathbf{0.70}^{***}$	$\mathbf{0.74}^{***}$	$\mathbf{-0.35}^{***}$	$\mathbf{0.11}^{***}$	1.00

grouped based on the data point density. In Fig. 6 and Table 4, it can be seen that the BTA, BTA-θ and BTA-Ca model groups had a satisfactory performance under various Ca ranges. The R^2 of the BTA, BTA-θ1, BTA-θ2, BTA-θ3, BTA-Ca1, BTA-Ca2 and BTA-Ca3 was 0.58 ~ 0.90, 0.69 ~ 0.94, 0.67 ~ 0.94, 0.70 ~ 0.94, 0.70 ~ 0.93, 0.69 ~ 0.94, 0.70 ~ 0.93, respectively. The BTA-θ and BTA-Ca model groups had a better performance when Ca was 320 ~ 360 cm^3/m^3 with the mean R^2 of 0.94, followed by 500 ~ 700 cm^3/m^3 with the mean R^2 of 0.92. Overall, it shows that high levels of CO_2 concentration inhibited ET and lowered the model accuracy just slightly.

3.3.3. *Evapotranspiration interannual variation and simple water balance*

The monthly mean ET was further calculated during the entire study period represented by the daily means in each calendar month. Fig. 7a demonstrates the clear seasonal variation of evapotranspiration, with high values in summer and autumn and low values in spring and winter. The highest ET appeared in late summer and early autumn (August and September) with the observed values of 3.11 ± 0.97 mm and 3.03 ± 0.97 mm, respectively. Further analysis and comparison show that the models (BTA, BTA-θ and BTA-Ca) slightly overestimated the winter ET and underestimated the autumn ET.

Moreover, the availability of water resources was assessed based on the difference between P and ET in Fig. 7b to evaluate the possible water surplus or shortage in each month over the four-year period. We observed that there were four months with clear water stress (January, October, November, December) mainly because of relatively low precipitation amount, whilst the water surplus occurred during spring and summer mostly during the rainy seasons. On average, the largest water surplus appeared in June (7.45 mm/d) and the largest water shortage appeared in October (-0.89 mm/d), and July saw the relative closure of the water balance at the study site. This characteristic of water resources availability can support well the plant growth during the growing seasons. However, it should be mentioned that the water shortage inferred here does not necessarily mean the trees are under water stress, because soil water storage was not included in this simple water balance calculation, which can be accessed by trees when precipitation was low.

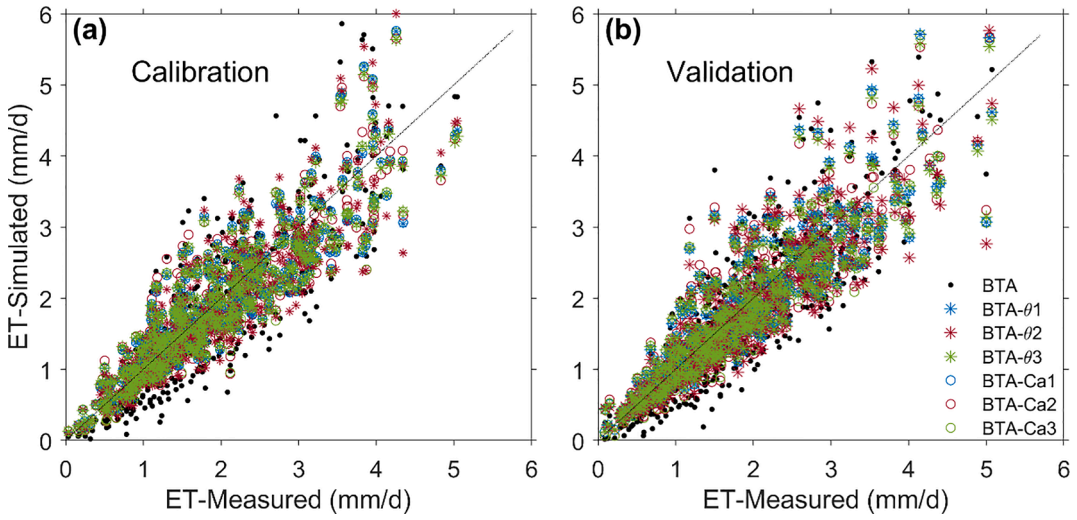

Fig. 4. Comparison of measured daily evapotranspiration against simulations by the BTA, BTA-θ and BTA-Ca model groups during (a) the calibration and (b) validation periods. Dotted lines are the 1:1 lines.

Table 3
Statistical results for ET comparisons between measurements and simulations. *s*: Slope of the linear regression; R^2: Linear regression coefficient of determination; *MAPE*: Mean absolute percentage error (%); *RMSE*: root mean square error (mm/d). Numbers in bold indicate the best performance in each model category; *BIC*: Bayesian information criterion.

Model	Calibration				Validation			
	R^2	*MAPE*	*RMSE*	*BIC*	R^2	*MAPE*	*RMSE*	*BIC*
BTA	0.73	27.51	0.60	−246.14	0.73	28.91	0.60	−247.23
BTA-θ1	0.81	19.05	0.43	−314.44	0.81	20.40	0.44	−307.42
BTA-θ2	0.79	20.38	0.48	−288.19	0.78	21.80	0.49	−278.39
BTA-θ3	**0.82**	**19.16**	**0.42**	**−316.9**	**0.81**	**20.66**	**0.43**	**−309.86**
BTA-Ca1	0.82	19.27	0.42	−320.96	0.82	20.62	0.42	−317.21
BTA-Ca2	0.82	19.23	0.42	−316.51	0.81	20.90	0.43	−310.7
BTA-Ca3	**0.82**	**18.76**	**0.41**	**−321.55**	**0.82**	**19.94**	**0.42**	**−318.53**

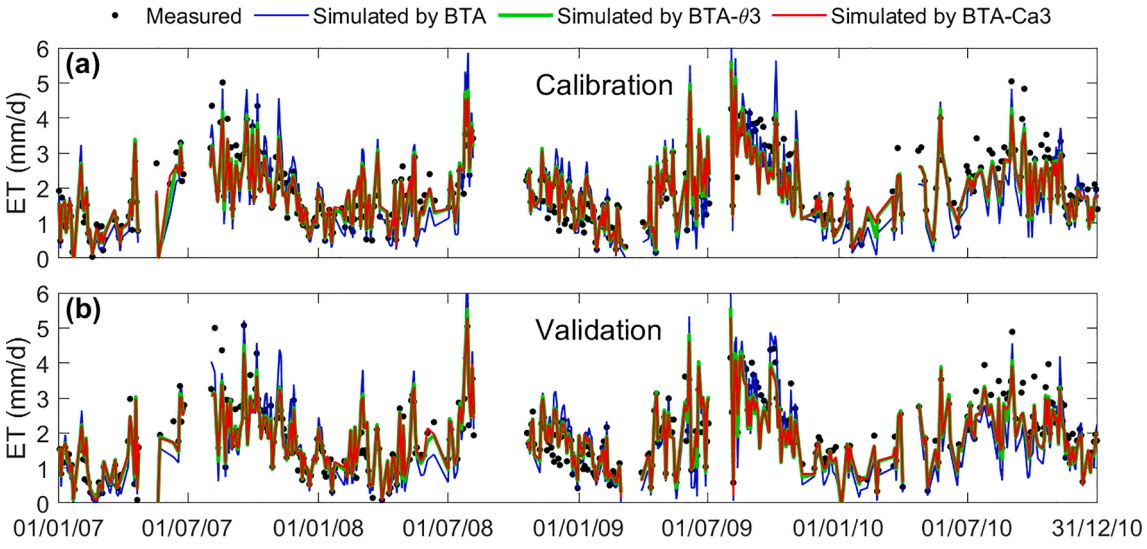

Fig. 5. Daily evapotranspiration simulated by BTA, BTA-θ3, and BTA-Ca3 with the for calibration and validation periods. The disconnected period indicates missing data.

4. Discussion

4.1. Impacts of environmental changes on water-carbon coupling

Environmental changes, such as radiation, wind speed, precipitation, relative humidity, sunshine duration, and temperature, play an important role in the dynamic changes of evapotranspiration, but their impacts often vary with location and climate. For example, net radiation was regarded the most influential variable in the North American temperate and boreal ecosystems (Isabelle et al., 2021), while

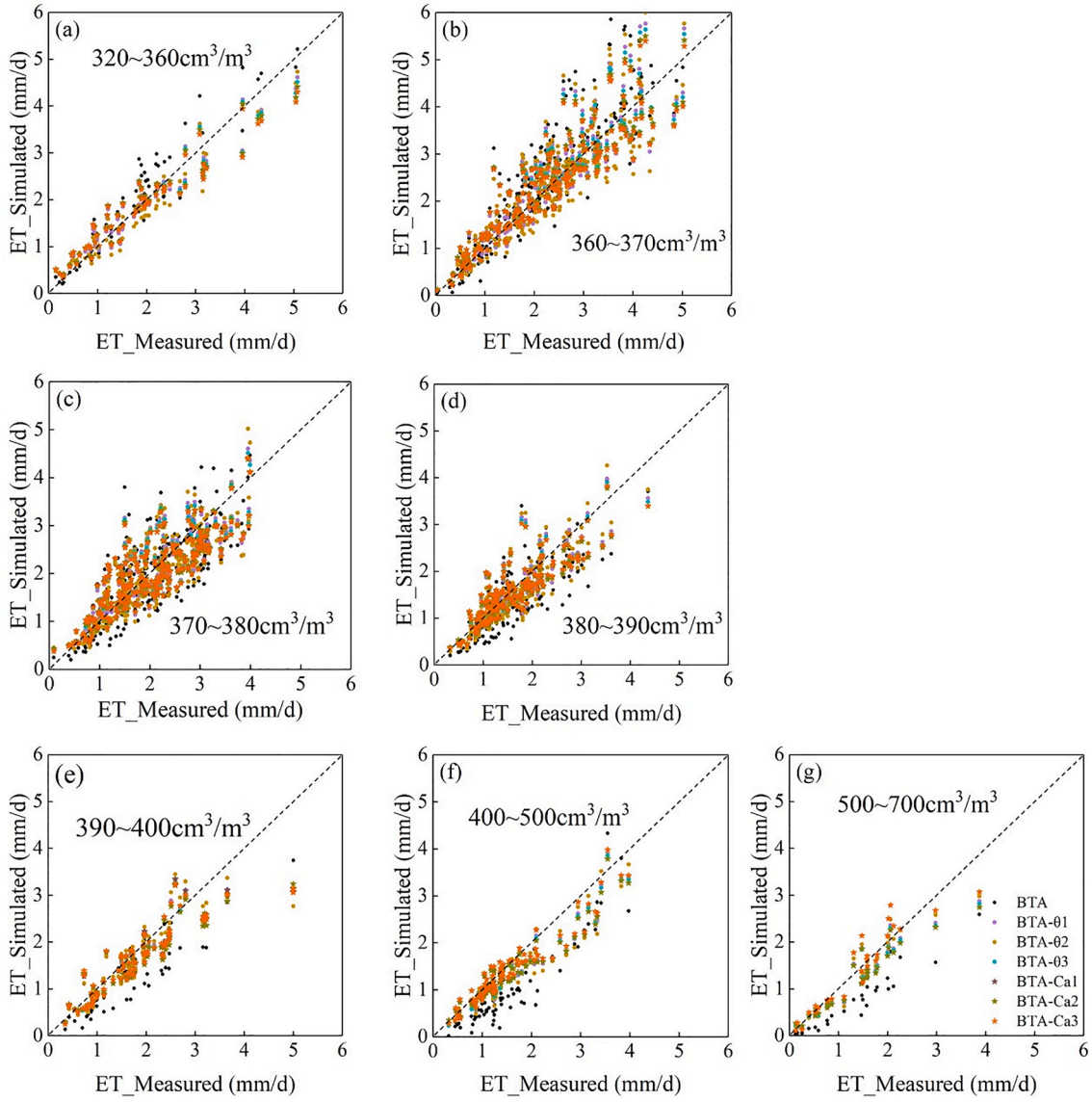

Fig. 6. Comparison of measured daily evapotranspiration against simulations by the BTA, BTA-θ and BTA-Ca model groups under different Ca levels. Dotted lines are the 1:1 lines. The Ca horizontal range is divided according to the density of the sample data.

Table 4
A comparison of the ET values simulated by the BTA, BTA-θ and BTA-Ca model groups under different Ca levels (cm^3/m^3). The comparison results are represented by R^2 (linear regression coefficient of determination).

Model	Ca						
	320 ~ 360	360 ~ 370	370 ~ 380	380 ~ 390	390 ~ 400	400 ~ 500	500 ~ 700
BTA	0.90	0.80	0.58	0.60	0.75	0.83	0.89
BTA-θ1	0.94	0.81	0.69	0.73	0.82	0.91	0.92
BTA-θ2	0.94	0.75	0.67	0.71	0.78	0.87	0.91
BTA-θ3	0.94	0.82	0.70	0.74	0.83	0.92	0.92
BTA-Ca1	0.93	0.82	0.70	0.74	0.83	0.91	0.91
BTA-Ca2	0.93	0.82	0.69	0.73	0.83	0.92	0.94
BTA-Ca3	0.93	0.82	0.70	0.74	0.83	0.92	0.91

precipitation was the predominant variable in the central Loess Plateau of China which is characterized by the warm temperate continental climate (L. Li et al., 2020). Wind speed was considered to be a controlling variable in some areas of south-western and north-western China (Li et al., 2014; Liu and Zhang, 2013), on the Canadian Prairies (Burn and Hesch, 2007) and in Iran (Dinpashoh et al., 2011). Temperature was found the dominant factor affecting ET in Xilingol League of China (Yu et al., 2020) and in Tropical Africa (Legesse et al., 2003). In addition, the atmospheric CO_2 concentration acts as the dominant factor controlling ET changes over the North America, South America and part of Asia (Shi et al., 2013). In our humid subtropical forest site, solar radiation was demonstrated the most influential variable for both ET and GPP, which was consistent with the results of many other studies such as Liu et al., (2017), followed by water vapor pressure deficit.

In an area like the Dinghushan forest watershed where water and carbon are sufficient (Liu et al., 2013), ET and GPP should not be limited by water supply but can be limited by radiation energy. Our study shows that solar radiation had a great influence on ET and GPP dynamics, and increases in solar radiation led to increases in ET and GPP, consistent with other studies in similar environments (Isabelle et al., 2021; Montaldo et al., 2020). As a main driver of evapotranspiration, solar

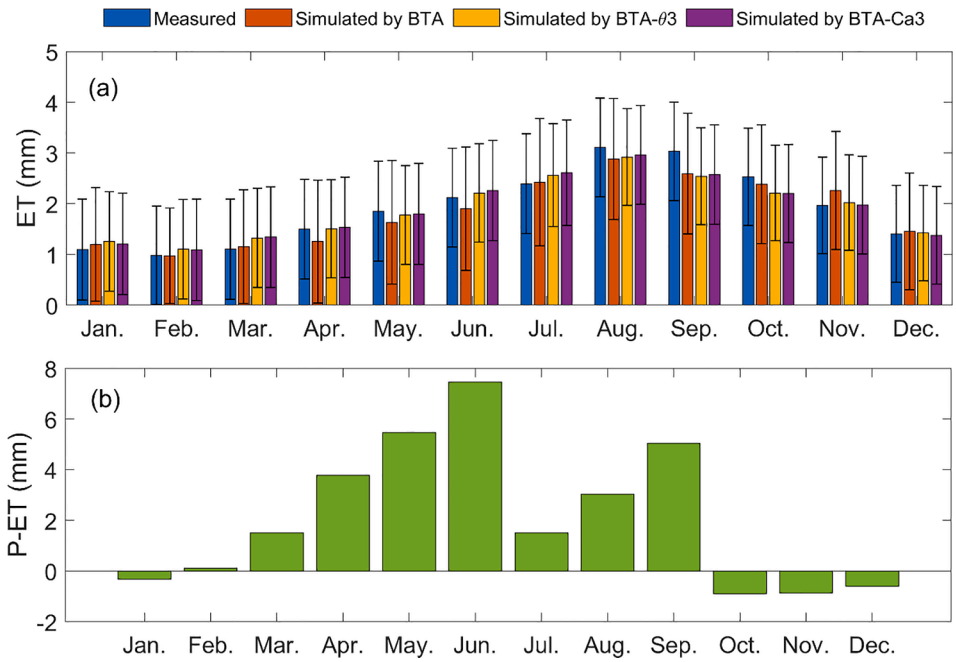

Fig. 7. (a) Monthly evapotranspiration simulated by BTA, BTA-θ3 and BTA-Ca3 during the entire period was compared with the observed values. Data were averaged to daily values for comparison; (b) simple water balance indicated by monthly difference between precipitation and evapotranspiration.

radiation can explain 55% of the daily variation in ET. The dominant role of solar radiation in ET changes was also discussed at a larger scale using satellite products in an extended wet humid area (Wang et al., 2021). Vapor pressure deficit was the second most important meteorological factor influencing ET. This is because the heat required for evapotranspiration mainly comes from solar radiation, while the driving force for the diffusion of water vapor to the atmosphere is mainly the difference in water vapor saturation status (Fan et al., 2004). Similar to water vapor flux (ET), the terrestrial ecosystem GPP from 2007 to 2010 was also strongly correlated with solar radiation, vapor pressure deficit and carbon dioxide concentration. Understandably, plant photosynthesis only occurs in environments with sufficient photosynthetic active radiation (PAR). The annual GPP in the old-growth subtropical forest was quite steady and presented relatively limited inter-annual variation (1430 ± 87 g C/m^2) (Liu et al., 2017; Yan et al., 2013).

Apart from the above similarity, we also observed that the responses ET and GPP to meteorological variables showed slight differences. The correlation of ET-D was greater than that of GPP-D, while the correlation of ET-Ca was weaker than that of GPP-Ca. The impact of environmental changes especially the increasing carbon dioxide concentration on photosynthesis was greater than that on evapotranspiration in our site. The daily average carbon dioxide concentration can explain 14% of the variation in ET versus 26% of the variation in GPP, which means that this old-growth forest can still assimilate carbon for biomass production (Yan et al., 2013). Changes in the hydrological cycle and CO_2 fertilization have a positive interaction, leading to a higher rate of carbon sequestration (Nemani et al., 2002). These findings infer that the forests will play an important and irreplaceable role in mitigating climate change impact as a carbon sink in most time of a year, especially in an environment where the CO_2 concentration is increasing gradually.

4.2. *The modified process-based model for evapotranspiration simulations*

The original BTA model did not take into account the change in soil water content which would presumably limit the performance of the model (Wang et al., 2016). By adding a soil water potential then a soil water content response function, Liu et al., (2019a, 2019b) improved the model for plant stomatal conductance and transpiration simulation. As a continuity, we further integrated the CO_2 concentration stress into the model, which gives it the capability to simulate water and carbon coupling processes. Additionally, we allowed one model parameter to vary with meteorological conditions by using ET_o which extends the model application from transpiration alone to total evapotranspiration estimates. In the semi-empirical multiplicative models, ET is the product of the response functions to individual factors, which sometimes need to consider the interactive effects between environmental factors (Damour et al., 2010). Our results showed that the modified models had a satisfactory performance in simulating the evapotranspiration of this subtropical forest. Our final model integrates the effects of both the major atmospheric conditions and the water supply conditions, as such, improvement of the simulation accuracy reflects well the underlying mechanisms of Ca effect on ET, for example, the restraint of CO_2 saturation on stomatal openness and thus ET. One possible reason for the limited difference between the BTA-θ model group and BTA-Ca model group can be that when the CO_2 concentration goes above a certain threshold (e.g., 350 cm^3/m^3), its limiting effect on stomata conductance will become stronger (i.e., f(Ca) < 1), which results in a reduction in ET rate inferred by the multiplicative structure of the model. Numerous studies have shown that lower Ca promotes stomatal opening, while higher Ca can induce stomatal closure (Ye et al., 2021; Zheng and Peng, 2003). Furthermore, regarding the effect of Ca on ET, there are two contrasting views that on the one hand, with the increase in Ca the leaf stomates will be closed or partially closed due to intercellular CO_2 saturation which then reduces the passing-through rate of water vapor, i.e., ET will be reduced with high Ca (Alkama et al., 2010; Betts et al., 2007; Cramer et al., 2001; Gedney et al., 2006); on the other hand, with the increase in Ca photosynthesis will be enhanced to produce more biomass that leaf area index (LAI) will therefore increase, and ET is usually positively associated with LAI (Cao et al., 2010; Felzer et al., 2009; Piao et al., 2007; Shi et al., 2013). As such, the positively effect of Ca on ET may be often observed at a relatively low Ca level in a long term such as seasonal or yearly analysis (Niemand et al., 2005; Piao et al., 2015, 2007), whilst the negative effect may mainly be present in a short term such as daily analysis (Kang et al., 1995; Li et al., 2003; Zhang et al., 1999).

4.3. Implications for forest water budget assessment under climate change

The current global atmospheric CO_2 concentration has increased significantly compared with pre-industrialization concentrations, with the average surface temperature increasing mainly due to the emission of CO_2 and other greenhouse gases. Climate change is exacerbating the water cycle, which was reported to result in more intense rains and floods, and also more severe droughts in many areas (IPCC, 2021). Climate extremes such as droughts and heatwaves have a large impact on terrestrial carbon uptake by reducing gross primary production (Gampe et al., 2021). Forests and their spatial distributions have always been considered an effective way to mitigate the global warming impacts (Kulmala et al., 2004; Zheng et al., 2022), because trees can absorb CO_2 in the air through photosynthesis and return water to the air via transpiration and interception loss (Macdicken et al., 2015). The increase in forest cover can assimilate more carbon dioxide but it can also lead to more water uptake, leaving less water for other users in the forest ecosystem. Therefore, ET estimation over forests considering CO_2 concentration is critical and urgent to explore the balance between carbon assimilation and water consumption. This study provides a simple example of coupling water and carbon, and can potentially be applied to assess the interactions between CO_2 and evaporative fluxes in other terrestrial ecosystems, even though the suitability of the stress function f (Ca) and its associated CO_2 concentration thresholds are worth further investigation to fit in different sites.

Moreover, through simple water balance calculations, we found that the forest in our site has grown in a relatively water-surplus environment in most time of the year, with water deficit primarily occurring in winter. However, this water deficit can be leveraged by the soil water and groundwater storage accumulated in summer and autumn prior to reduced precipitation in winter. In addition, because of the high vegetation density in the old-growth forest stand dominated by monsoon evergreen broad-leaved forest (MBF) with a LAI of 4.9 ~ 5.6 throughout the year, it is assumed that the total ET in the site is mostly attributed to plant transpiration although the proportion cannot be quantified without concurrent sap flow measurements. The transpiration-to-evapotranspiration ratio is a key parameter to quantify ecosystem water use efficiency and important to assist forest water management. The ratio can be affected by both environmental factors (e.g., solar radiation, air temperature, air humidity, precipitation, wind speed, soil moisture content) and biological factors (e.g., vegetation types and canopy cover, and LAI) (Gu et al., 2018; Nelson et al., 2020). It is worth mentioning that when Jarvis (1976) developed an empirical transpiration model, LAI was present, however, due to its gradual change characteristics and often low measuring frequency compared to other environmental factors, LAI was neglected in the development afterwards. Ren et al., (2019) estimated that the ratio of the evergreen broadleaf forests in the humid south China was as high as 0.8, higher than other plant functional types including deciduous broadleaf forest and evergreen needleleaf forest, etc. Therefore, the ET simulated by the modified models in this study can capture the water availability dynamics well, which indicates that our model can serve as a useful tool in the humid subtropical forests to examine the water budget at a fine temporal scale.

5. Conclusions

By considering the effects of climate change (e.g., the increase of carbon dioxide concentration), we constructed and integrated a Ca stress function into a simplified process-based transpiration model. Using the meteorological data of Dinghushan Ecological Reserve from 2007 to 2010, we compared the original and two modified model groups. Results showed that these models had agreeable simulation results in a subtropical forest. Both modified models performed better than the original one, and their applications in evapotranspiration estimation were sound and robust. The insignificant difference in model performance where different types of soil water content stress functions were tested may suggest the weak role of soil water content in evaporation process in this region due to the high saturation conditions. An overall negative relationship between daily Ca and ET was found, and a threshold of Ca at 350 cm^3/m^3 was observed for this site above which ET will decrease, but this threshold can vary with different study sites and needs further verification. The positive effect of Ca on ET can occur in long-term study like annual analysis, which is not observed here for daily scale analysis. In the context of climate change, predicting how the increase of Ca will affect hydrologic processes including evapotranspiration is crucial for an extensive range of applications, and this study provides a tool for prediction of forest evapotranspiration towards an improved understanding of water-carbon coupling processes.

CRediT authorship contribution statement

Meiting Liu: Conceptualization, Methodology, Formal analysis, Writing – original draft. **Hailong Wang:** Conceptualization, Writing – review & editing, Supervision, Funding acquisition. **Xiaodong Liu:** Data curation, Resources, Writing – review & editing. **Bingjun Liu:** . **Xiaohong Chen:** Writing – review & editing. **Qianmei Zhang:** Data curation, Investigation. **Ze Meng:** Data curation, Investigation.

Declaration of Competing Interest

The authors declare that they have no known competing financial interests or personal relationships that could have appeared to influence the work reported in this paper.

Data availability

Data will be made available on request.

Acknowledgements

This study is supported by the the National Natural Science Foundation of China (42171020), the Guangdong Provincial Department of Science and Technology, China (2019ZT08G090), and the Forestry Science and Technology Innovation Project of Guangdong Province (2021KJCX003 and 2021-KYXM-09). We gratefully acknowledge the data support of the Dinghushan Forest Ecosystem Research Station. We thank the Editor and anonymous reviewers for their invaluable comments and suggestion to improve the quality of the paper.

References

Ala-aho, P., Soulsby, C., Wang, H., Tetzlaff, D., 2017. Integrated surface-subsurface model to investigate the role of groundwater in headwater catchment runoff generation: A minimalist approach to parameterisation. J. Hydrol. 547, 664–677. https://doi.org/10.1016/j.jhydrol.2017.02.023.

Alkama, R., Cescatti, A., 2016. Biophysical climate impacts of recent changes in global forest cover. Science 351 (6273), 600–604.

Alkama, R., Kageyama, M., Ramstein, G., 2010. Relative contributions of climate change, stomatal closure, and leaf area index changes to 20th and 21st century runoff change: A modelling approach using the Organizing Carbon and Hydrology in Dynamic Ecosystems (ORCHIDEE) land surface model. J. Geophys. Res. Atmos. 115, 1–9. https://doi.org/10.1029/2009JD013408.

Allen, R.G., Pereira, L.S., Howell, T.A., Jensen, M.E., 2011. Evapotranspiration information reporting: I. Factors governing measurement accuracy. Agric. Water Manag. 98 (6), 899–920. https://doi.org/10.1016/j.agwat.2010.12.015.

Anderson, M., Norman, J., Kustas, W., Houborg, R., Starks, P., Agam, N., 2008. A thermal-based remote sensing technique for routine mapping of land-surface carbon, water and energy fluxes from field to regional scales. Remote Sens. Environ. 112 (12), 4227–4241. https://doi.org/10.1016/j.rse.2008.07.009.

Baldocchi, D., Falge, E., Gu, L., Olson, R., Hollinger, D., Running, S., Anthoni, P., Bernhofer, C., Davis, K., Evans, R., Fuentes, J., Goldstein, A., Katul, G., Law, B., Lee, X., Malhi, Y., Meyers, T., Munger, W., Oechel, W., Paw, U.K.T., Pilegaard, K., Schmid, H.P., Valentini, R., Verma, S., Vesala, T., Wilson, K., Wofsy, S., 2001. FLUXNET: A new tool to study the temporal and spatial variability of ecosystem-scale carbon dioxide, water vapor, and energy flux densities. Bull. Am. Meteorol. Soc. 82, 2415–2434. https://doi.org/10.1175/1520-0477(2001)082<2415:FANTTS>2.3.CO;2.

Bernacchi, C.J., Kimball, B.A., Quarles, D.R., Long, S.P., Ort, D.R., 2007. Decreases in stomatal conductance of soybean under open-air elevation of [CO2] are closely coupled with decreases in ecosystem evapotranspiration. Plant Physiol. 143, 134–144. https://doi.org/10.1104/pp.106.089557.

Betts, R.A., Boucher, O., Collins, M., Cox, P.M., Falloon, P.D., Gedney, N., Hemming, D. L., Huntingford, C., Jones, C.D., Sexton, D.M.H., Webb, M.J., 2007. Projected increase in continental runoff due to plant responses to increasing carbon dioxide. Nature 448 (7157), 1037–1041. https://doi.org/10.1038/nature06045.

Buckley, T.N., Mott, K.A., Farquhar, G.D., 2003. A hydromechanical and biochemical model of stomatal conductance. Plant, Cell Environ. 26, 1767–1785. https://doi.org/10.1046/j.1365-3040.2003.01094.x.

Buckley, T.N., Turnbull, T.L., Adams, M.A., 2012. Simple models for stomatal conductance derived from a process model: Cross-validation against sap flux data. Plant Cell Environ. 35, 1647–1662. https://doi.org/10.1111/j.1365-3040.2012.02515.x.

Burn, D.H., Hesch, N.M., 2007. Trends in evaporation for the Canadian Prairies. J. Hydrol. 336 (1-2), 61–73.

Busscher, WARREN, 1980. Simulation of field water use and crop yield. Soil Sci. 129 (3), 193. https://doi.org/10.1097/00010694-198003000-00016.

Cao, L., Bala, G., Caldeira, K., Nemani, R., Ban-Weiss, G., 2010. Importance of carbon dioxide physiological forcing to future climate change. Proc. Natl. Acad. Sci. U. S. A. 107 (21), 9513–9518. https://doi.org/10.1073/pnas.0913000107.

Cramer, W., Bondeau, A., Woodward, F.I., Prentice, I.C., Betts, R.A., Brovkin, V., Cox, P. M., Fisher, V., Foley, J.A., Friend, A.D., Kucharik, C., Lomas, M.R., Ramankutty, N., Sitch, S., Smith, B., White, A., Young-Molling, C., 2001. Global response of terrestrial ecosystem structure and function to CO2 and climate change: results from six dynamic global vegetation models. Glob. Chang. Biol. 7, 357–373. 10.1046/j.1365-2486.2001.00383.x.

Cristea, N.C., Kampf, S.K., Burges, S.J., 2013. Revised coefficients for Priestley-Taylor and Makkink-Hansen equations for estimating daily reference evapotranspiration. J. Hydrol. Eng. 18 (10), 1289–1300. https://doi.org/10.1061/(ASCE)HE.1943-5584.0000679.

Damour, G., Simonneau, T., Cochard, H., Urban, L., 2010. An overview of models of stomatal conductance at the leaf level. Plant, Cell Environ. 33, 1419–1438. https://doi.org/10.1111/j.1365-3040.2010.02181.x.

Dinpashoh, Y., Jhajharia, D., Fakheri-Fard, A., Singh, V.P., Kahya, E., 2011. Trends in reference crop evapotranspiration over Iran. J. Hydrol. 399 (3-4), 422–433.

Fan, A., Liu, W., Wang, C., 2004. Effects of environmental factors on the evapotranspiration of the soil water. Acta Energiae Solaris Sin. 25 (1), 1–5.

Federer, C.A., 1979. A soil-plant-atmosphere model for transpiration and availability of soil water. Water Resour. Res. 15, 555–562. 10.1029/WR015i003p00555.

Felzer, B.S., Cronin, T.W., Melillo, J.M., Kicklighter, D.W., Adam Schlosser, C., 2009. Importance of carbon-nitrogen interactions and ozone on ecosystem hydrology during the 21st century. J. Geophys. Res. Biogeosciences 114, 1–10. https://doi.org/10.1029/2008JG000826.

Fisher, J.B., Melton, F., Middleton, E., Hain, C., Anderson, M., Allen, R., McCabe, M.F., Hook, S., Baldocchi, D., Townsend, P.A., Kilic, A., Tu, K., Miralles, D.D., Perret, J., Lagouarde, J.-P., Waliser, D., Purdy, A.J., French, A., Schimel, D., Famiglietti, J.S., Stephens, G., Wood, E.F., 2017. The future of evapotranspiration: Global requirements for ecosystem functioning, carbon and climate feedbacks, agricultural management, and water resources. Water Resour. Res. 53 (4), 2618–2626.

Gampe, D., Zscheischler, J., Reichstein, M., O'Sullivan, M., Smith, W.K., Sitch, S., Buermann, W., 2021. Increasing impact of warm droughts on northern ecosystem productivity over recent decades. Nat. Clim. Chang. 11 (9), 772–779. https://doi.org/10.1038/s41558-021-01112-8.

Gao, Q., Zhao, P., Zeng, X., Cai, X., Shen, W., 2002. A model of stomatal conductance to quantify the relationship between leaf transpiration, microclimate and soil water stress. Plant, Cell Environ. 25, 1373–1381. https://doi.org/10.1046/j.1365-3040.2002.00926.x.

Garcia, M., Sandholt, I., Ceccato, P., Ridler, M., Mougin, E., Kergoat, L., Morillas, L., Timouk, F., Fensholt, R., Domingo, F., 2013. Actual evapotranspiration in drylands derived from in-situ and satellite data: Assessing biophysical constraints. Remote Sens. Environ. 131, 103–118. https://doi.org/10.1016/j.rse.2012.12.016.

Gedney, N., Cox, P.M., Betts, R.A., Boucher, O., Huntingford, C., Stott, P.A., 2006. Detection of a direct carbon dioxide effect in continental river runoff records. Nature 439 (7078), 835–838. https://doi.org/10.1038/nature04504.

Gopalakrishnan, R., Bala, G., Jayaraman, M., Cao, L., Nemani, R., Ravindranath, N.H., 2011. Sensitivity of terrestrial water and energy budgets to CO2-physiological forcing: An investigation using an offline land model. Environ. Res. Lett. 6 (4), 044013. https://doi.org/10.1088/1748-9326/6/4/044013.

Greve, P., Orlowsky, B., Mueller, B., Sheffield, J., Reichstein, M., Seneviratne, S.I., 2014. Global assessment of trends in wetting and drying over land. Nat. Geosci. 7 (10), 716–721.

Gu, C., Ma, J., Zhu, G., Yang, H., Zhang, K., Wang, Y., Gu, C., 2018. Partitioning evapotranspiration using an optimized satellite-based ET model across biomes. Agric. For. Meteorol. 259, 355–363. https://doi.org/10.1016/j.agrformet.2018.05.023.

Guan, H., Zhang, X., Makhnin, O., Sun, Z., 2013. Mapping mean monthly temperatures over a coastal hilly area incorporating terrain aspect effects. J. Hydrometeorol. 14, 233–250. https://doi.org/10.1175/JHM-D-12-014.1.

Guyot, A., Fan, J., Oestergaard, K.T., Whitley, R., Gibbes, B., Arsac, M., Lockington, D.A., 2017. Soil-water content characterisation in a modified Jarvis-Stewart model: A case study of a conifer forest on a shallow unconfined aquifer. J. Hydrol. 544, 242–253. https://doi.org/10.1016/j.jhydrol.2016.11.041.

Shwetha, H.R., Kumar, D.N., 2015. Prediction of land surface temperature under cloudy conditions using microwave remote sensing and ANN. Aquat. Procedia 4, 1381–1388. https://doi.org/10.1016/j.aqpro.2015.02.179.

Hargreaves, G.H., Samani, Z.A., 1982. Estimating potential evapotranspiration. J. Irrig. Drain. Div. - ASCE 108 (3), 225–230. https://doi.org/10.1061/JRCEA4.0001390.

Hawkins, D.M., 2004. The Problem of Overfitting. J. Chem. Inf. Comput. Sci. 44 (1), 1–12.

Held, I.M., Soden, B.J., 2006. Robust responses of the hydrological cycle to global warming. J. Clim. 19, 5686–5699.

Huntington, T.G., 2006. Evidence for intensification of the global water cycle: Review and synthesis. J. Hydrol. 319 (1-4), 83–95. https://doi.org/10.1016/j.jhydrol.2005.07.003.

Hussain, M.Z., VanLoocke, A., Siebers, M.H., Ruiz-Vera, U.M., Cody Markelz, R.J., Leakey, A.D.B., Ort, D.R., Bernacchi, C.J., 2013. Future carbon dioxide concentration decreases canopy evapotranspiration and soil water depletion by field-grown maize. Glob. Chang. Biol. 19, 1572–1584. 10.1111/gcb.12155.

IPCC, 2021. Summary for Policymakers. In: Climate Change 2021: The Physical Science Basis. Contribution of Working Group I to the Sixth Assessment Report of the Intergovernmental Panel on Climate Change. Cambridge Univ. Press In Press.

Isabelle, P.-E., Viens, L., Nadeau, D.F., Anctil, F., Wang, J., Maheu, A., 2021. Sensitivity analysis of the maximum entropy production method to model evaporation in boreal and temperate forests. Geophys. Res. Lett. 48 (13) https://doi.org/10.1029/2020GL091919.

Jarvis, P.G., 1976. The interpretation of the variations in leaf water potential and stomatal conductance found in canopies in the field. Philos. Trans. R. Soc. London. B. Biol. Sci. 273, 593–610. https://doi.org/10.1098/rstb.1976.0035.

Kang, S., Cai, H., Liu, X., 1995. Effects of CO2 enrichment, nitrogen and water on photosynthesis, evapotranspiration and water use efficiency of spring wheat. Acta Univ Agric Boreali-Occidentalis 23, 1–5.

Kothavala, Z., Arain, M.A., Black, T.A., Verseghy, D., 2005. The simulation of energy, water vapor and carbon dioxide fluxes over common crops by the Canadian Land Surface Scheme (CLASS). The simulation of energy, water vapor and carbon dioxide fluxes over common crops by the Canadian Land Surface Scheme (CLASS) 133 (1-4), 89–108. https://doi.org/10.1016/j.agrformet.2005.08.007.

Kruijt, B., Witte, J.-P., Jacobs, C.M.J., Kroon, T., 2008. Effects of rising atmospheric CO2 on evapotranspiration and soil moisture: A practical approach for the Netherlands. J. Hydrol. 349 (3-4), 257–267. https://doi.org/10.1016/j.jhydrol.2007.10.052.

Kulmala, M., Suni, T., Lehtinen, K.E.J., Dal Maso, M., Boy, M., Reissell, A., Rannik, Ü., Aalto, P., Keronen, P., Hakola, H., Bäck, J., Hoffmann, T., Vesala, T., Hari, P., 2004. A new feedback mechanism linking forests, aerosols, and climate. Atmos. Chem. Phys. 4, 557–562. https://doi.org/10.5194/acp-4-557-2004.

Legesse, D., Vallet-Coulomb, C., Gasse, F., 2003. Hydrological response of a catchment to climate and land use changes in Tropical Africa: case study South Central Ethiopia. J. Hydrol. 275 (1-2), 67–85. https://doi.org/10.1016/S0022-1694(03)00019-2.

Li, F., Kang, S., Zhang, F., 2003. Effects of CO2 enrichment, nitrogen and water on photosynthesis, evapotranspiration and water use efficiency of spring wheat. Chinese J. Appl. Ecol. 14, 387–393.

Li, L., Song, X., Xia, L.u., Fu, N.a., Feng, D., Li, H., Li, Y., 2020a. Modelling the effects of climate change on transpiration and evaporation in natural and constructed grasslands in the semi-arid Loess Plateau. China. Agric. Ecosyst. Environ. 302, 107077. https://doi.org/10.1016/j.agee.2020.107077.

Li, Y., Yan, J., Meng, Z., Huang, J., Zhang, L., Chen, Z., Liu, S., Zhang, Q., Zhang, D., 2020b. An observation dataset of carbon and water fluxes in a mixed coniferous broad-leaved forest at Dinghushan, Southern China (2003-2010). Sci. Data Bank. https://doi.org/10.11922/sciencedb.1009.

Li, Z., Chen, Y., Yang, J., Wang, Y., 2014. Potential evapotranspiration and its attribution over the past 50years in the arid region of Northwest China. Hydrol. Process. 28, 1025–1031. https://doi.org/10.1002/hyp.9643.

Liao, D., Niu, J., Kang, S., Singh, S.K., Du, T., 2021. Effects of elevated CO2 on the evapotranspiration over the agricultural land in Northwest China. J. Hydrol. 593, 125858. https://doi.org/10.1016/j.jhydrol.2020.125858.

Liu, J., You, Y., Li, J., Sitch, S., Gu, X., Nabel, J.E.M.S., Lombardozzi, D., Luo, M., Feng, X., Arneth, A., Jain, A.K., Friedlingstein, P., Tian, H., Poulter, B., Kong, D., 2021. Response of global land evapotranspiration to climate change, elevated CO2, and land use change. Agric. For. Meteorol. 311, 108663. https://doi.org/10.1016/j.agrformet.2021.108663.

Liu, N.a., Buckley, T.N., He, X., Zhang, X., Zhang, C., Luo, Z., Wang, H., Sterling, N., Guan, H., 2019a. Improvement of a simplified process-based model for estimating transpiration under water-limited conditions. Hydrol. Process. 33 (12), 1670–1685. https://doi.org/10.1002/hyp.13430.

Liu, N.a., Wang, H., He, X., Deng, Z., Zhang, C., Zhang, X., Guan, H., 2019b. A hybrid transpiration model for water-limited conditions. J. Hydrol. 578, 124104. https://doi.org/10.1016/j.jhydrol.2019.124104.

Liu, X., Chen, X., Li, R., Long, F., Zhang, L.u., Zhang, Q., Li, J., 2017. Water-use efficiency of an old-growth forest in lower subtropical China. Sci. Rep. 7 (1) https://doi.org/10.1038/srep42761.

Liu, X., Li, Y., Chen, X., Zhou, G., Cheng, J., Zhang, D., Meng, Z.e., Zhang, Q., 2015. Partitioning evapotranspiration in an intact forested watershed in southern China. Ecohydrology 8 (6), 1037–1047. https://doi.org/10.1002/eco.1561.

Liu, X., Zhang, D., 2013. Trend analysis of reference evapotranspiration in northwest china: The roles of changing wind speed and surface air temperature. Hydrol. Process. 27 (26), 3941–3948. https://doi.org/10.1002/hyp.9527.

Liu, X., Zhang, D., Meng, Z., Zhang, Q., Zhou, G., 2013. Dynamic features and mechanisms of shallow groundwater in the downstream of Dinghushan Biosphere Reserve[J]. Ecol. Sci. 32, 137–143. https://doi.org/10.3969/j.issn.

Lovelli, S., Perniola, M., Di Tommaso, T., Ventrella, D., Moriondo, M., Amato, M., 2010. Effects of rising atmospheric CO2 on crop evapotranspiration in a Mediterranean area. Agric. Water Manag. 97 (9), 1287–1292. https://doi.org/10.1016/j.agwat.2010.03.005.

Macdicken, K., Fao, R., Jonsson, ., Pia, L., Maulo, S., Adikari, Y., Garzuglia, M., Lindquist, E., Reams, G., D'Annunzio, R., 2015. Global forest resources assessment 2015: How are the world's forests changing? FAO 244.

Mallick, K., Trebs, I., Boegh, E., Giustarini, L., Schlerf, M., Drewry, D.T., Hoffmann, L., von Randow, C., Kruijt, B., Araùjo, A., Saleska, S., Ehleringer, J.R., Domingues, T.F., Ometto, J.P.H.B., Nobre, A.D., de Moraes, O.L.L., Hayek, M., Munger, J.W., Wofsy, S. C., 2016. Canopy-scale biophysical controls of transpiration and evaporation in the Amazon Basin. Hydrol. Earth Syst. Sci. 20 (10), 4237–4264. https://doi.org/10.5194/hess-20-4237-201610.5194/hess-20-4237-2016-supplement.

Milly, P.C.D., Dunne, K.A., 2017. A hydrologic drying bias in water-resource impact analyses of anthropogenic climate change. J. Am. Water Resour. Assoc. 53 (4), 822–838. https://doi.org/10.1111/1752-1688.12538.

Montaldo, N., Curreli, M., Corona, R., Oren, R., 2020. Fixed and variable components of evapotranspiration in a Mediterranean wild-olive - grass landscape mosaic. Agric. For. Meteorol. 280, 107769.

Monteith, J.I.L., 1965. Evaporation and environment. Symp. Soc. Exp. Biol. 19, 205–234.

Nelson, J.A., Pérez-Priego, O., Zhou, S., Poyatos, R., Zhang, Y., Blanken, P.D., Gimeno, T. E., Wohlfahrt, G., Desai, A.R., Gioli, B., Limousin, J.-M., Bonal, D., Paul-Limoges, E., Scott, R.L., Varlagin, A., Fuchs, K., Montagnani, L., Wolf, S., Delpierre, N., Berveiller, D., Gharun, M., Belelli Marchesini, L., Gianelle, D., Šigut, L., Mammarella, I., Siebicke, L., Andrew Black, T., Knohl, A., Hörtnagl, L., Magliulo, V., Besnard, S., Weber, U., Carvalhais, N., Migliavacca, M., Reichstein, M., Jung, M., 2020. Ecosystem transpiration and evaporation: Insights from three water flux partitioning methods across FLUXNET sites. Glob. Chang. Biol. 26 (12), 6916–6930. https://doi.org/10.1111/gcb.15314.

Nemani, R., White, M., Thornton, P., Nishida, K., Reddy, S., Jenkins, J., Running, S., 2002. Recent trends in hydrologic balance have enhanced the terrestrial carbon sink in the United States. Geophys. Res. Lett. 29 (10), 106-1.

Niemand, C., Köstner, B., Prasse, H., Grünwald, T., Bernhofer, C., 2005. Relating tree phenology with annual carbon fluxes at Tharandt forest. Meteorol. Zeitschrift 14 (2), 197–202. https://doi.org/10.1127/0941-2948/2005/0022.

Oki, T., Kanae, S., 2006. Global hydrological cycles and world water resources. Science 313 (5790), 1068–1072.

Pascolini-Campbell, M., Reager, J.T., Chandanpurkar, H.A., Rodell, M., 2021. A 10 per cent increase in global land evapotranspiration from 2003 to 2019. Nature 593, 543–547. https://doi.org/10.1038/s41586-021-03503-5.

Piao, S., Friedlingstein, P., Ciais, P., de Noblet-Ducoudré, N., Labat, D., Zaehle, S., 2007. Changes in climate and land use have a larger direct impact than rising CO2 on global river runoff trends. Proc. Natl. Acad. Sci. U. S. A. 104 (39), 15242–15247. https://doi.org/10.1073/pnas.0707213104.

Piao, S., Yin, G., Tan, J., Cheng, L., Huang, M., Li, Y., Liu, R., Mao, J., Myneni, R.B., Peng, S., Poulter, B., Shi, X., Xiao, Z., Zeng, N., Zeng, ZhenZhong, Wang, Y., 2015. Detection and attribution of vegetation greening trend in China over the last 30 years. Glob. Chang. Biol. 21 (4), 1601–1609. https://doi.org/10.1111/gcb.12795.

Priestley, C.H.B., Taylor, R.J., 1972. On the assessment of surface heat flux and evaporation using large-scale parameters. Mon. Weather Rev. 100, 81–92. https://doi.org/10.1175/1520-0493(1972)100<0081:otaosh>2.3.co;2.

Ren, X., Lu, Q., He, H., Zhang, L., Niu, Z., 2019. Spatio-temporal variations of the ratio of transpiration to evapotranspiration in forest ecosystems along the North-South Transect of Eastern China. Dili Xuebao/Acta Geogr. Sin. 74, 63–75. https://doi.org/10.11821/dlxb201901005.

Schwarz, G., 1978. Estimating the dimension of a model. Ann. Stat. 6, 461–464.

Scott, R.L., James Shuttleworth, W., Goodrich, D.C., Maddock, T., 2000. The water use of two dominant vegetation communities in a semiarid riparian ecosystem. Agric. For. Meteorol. 105, 241–256. https://doi.org/10.1016/S0168-1923(00)00181-7.

Seiller, G., Anctil, F., 2016. How do potential evapotranspiration formulas influence hydrological projections? Hydrol. Sci. J. 61 (12), 2249–2266. https://doi.org/10.1080/02626667.2015.1100302.

Shi, X., Mao, J., Thornton, P.E., Huang, M., 2013. Spatiotemporal patterns of evapotranspiration in response to multiple environmental factors simulated by the Community Land Model. Environ. Res. Lett. 8 (2), 024012. https://doi.org/10.1088/1748-9326/8/2/024012.

Sitch, S., Huntingford, C., Gedney, N., Levy, P.E., Lomas, M., Piao, S.L., Betts, R., Ciais, P., Cox, P., Friedlingstein, P., Jones, C.D., Prentice, I.C., Woodward, F.I., 2008. Evaluation of the terrestrial carbon cycle, future plant geography and climate-carbon cycle feedbacks using five Dynamic Global Vegetation Models (DGVMs). Glob. Chang. Biol. 14, 2015–2039. https://doi.org/10.1111/j.1365-2486.2008.01626.x.

Stewart, J.B., 1988. Modelling surface conductance of pine forest. Agric. For. Meteorol. 43 (1), 19–35. https://doi.org/10.1016/0168-1923(88)90003-2.

Twine, T.E., Kustas, W.P., Norman, J.M., Cook, D.R., Houser, P.R., Meyers, T.P., Prueger, J.H., Starks, P.J., Wesely, M.L., 2000. Correcting eddy-covariance flux underestimates over a grassland. Agric. For. Meteorol. 103, 279–300. 10.1016/S0168-1923(00)00123-4.

Vrugt, J.A., 2016. Markov chain Monte Carlo simulation using the DREAM software package: Theory, concepts, and MATLAB implementation. Environ. Model. Softw. 75, 273–316. 10.1016/j.envsoft.2015.08.013.

Wang, H., Duan, K., Liu, B., Chen, X., 2021. Assessing the large-scale plant–water relations in the humid, subtropical Pearl River basin of China. Hydrol. Earth Syst. Sci. 25 (9), 4741–4758. https://doi.org/10.5194/hess-25-4741-202110.5194/hess-25-4741-2021-supplement.

Wang, H., Guan, H., Deng, Z., Simmons, C.T., 2014. Optimization of canopy conductance models from concurrent measurements of sap flow and stem water potential on Drooping Sheoak in South Australia. Water Resour. Res. 50, 6154–6167. 10.1002/2013WR014818.

Wang, H., Guan, H., Liu, N.a., Soulsby, C., Tetzlaff, D., Zhang, X., 2020. Improving the Jarvis-type model with modified temperature and radiation functions for sap flow simulations. J. Hydrol. 587, 124981. https://doi.org/10.1016/j.jhydrol.2020.124981.

Wang, H., Guan, H., Simmons, C.T., 2016. Modeling the environmental controls on tree water use at different temporal scales. Agric. For. Meteorol. 225, 24–35. 10.1016/j.agrformet.2016.04.016.

Wang, H., Tetzlaff, D., Soulsby, C., 2017. Testing the maximum entropy production approach for estimating evapotranspiration from closed canopy shrubland in a low-energy humid environment. Hydrol. Process. 31 (25), 4613–4621. https://doi.org/10.1002/hyp.11363.

Wang, J., Bras, R.L., 2011. A model of evapotranspiration based on the theory of maximum entropy production. Water Resour. Res. 47, 1–10. https://doi.org/10.1029/2010WR009392.

Wang, S., 2007. Simulation of evapotranspiration and its response to plant water and CO2 transfer dynamics 9, 426–443. https://doi.org/10.1175/2007JHM918.1.

Webb, E.K., Pearman, G.I., Leuning, R., 1980. Correction of flux measurments for density effects due to heat and water vapour transfer. Q. J. R. Meteorol. Soc. 106, 85–100.

Whitley, R., Taylor, D., Macinnis-Ng, C., Zeppel, M., Yunusa, I., O'Grady, A., Froend, R., Medlyn, B., Eamus, D., 2013. Developing an empirical model of canopy water flux describing the common response of transpiration to solar radiation and VPD across five contrasting woodlands and forests. Hydrol. Process. 27 (8), 1133–1146. https://doi.org/10.1002/hyp.9280.

Xiang, K., Li, Y.i., Horton, R., Feng, H., 2020. Similarity and difference of potential evapotranspiration and reference crop evapotranspiration – a review. Agric. Water Manag. 232, 106043. https://doi.org/10.1016/j.agwat.2020.106043.

Xie, S., Mo, X., Hu, S., Liu, S., 2020. Contributions of climate change, elevated atmospheric CO2 and human activities to ET and GPP trends in the Three-North Region of China. Agric. For. Meteorol. 295, 108183. https://doi.org/10.1016/j.agrformet.2020.108183.

Xu, D., Agee, E., Wang, J., Ivanov, V.Y., 2019. Estimation of Evapotranspiration of Amazon Rainforest Using the Maximum Entropy Production Method. Geophys. Res. Lett. 46 (3), 1402–1412. https://doi.org/10.1029/2018GL080907.

Xu, S., Yu, Z., Ji, X., Sudicky, E.A., 2017. Comparing three models to estimate transpiration of desert shrubs. J. Hydrol. 550, 603–615. https://doi.org/10.1016/j.jhydrol.2017.05.027.

Xu, S., Yu, Z., Zhang, K., Ji, X., Yang, C., Sudicky, E.A., 2018. Simulating canopy conductance of the Haloxylon ammodendron shrubland in an arid inland river basin of northwest China. Agric. For. Meteorol. 249, 22–34. https://doi.org/10.1016/j.agrformet.2017.11.015.

Yan, J., Zhang, Y., Yu, G., Zhou, G., Zhang, L., Li, K., Tan, Z., Sha, L., 2013. Seasonal and inter-annual variations in net ecosystem exchange of two old-growth forests in southern China. Agric. For. Meteorol. 182–183, 257–265. https://doi.org/10.1016/j.agrformet.2013.03.002.

Ye, H., Zhang, T., Yi, G., Li, J., Bie, X., Liu, D., Luo, L., 2018. Spatio-temporal characteristics of evapotranspiration and its relationship with climate factors in the source region of the Yellow River from 2000 to 2014. Dili Xuebao/Acta Geogr. Sin. 73, 2117–2134. https://doi.org/10.11821/dlxb201811006.

Ye, Z.P., Yu, F., An, T., Wang, F.B., Kang, H.J., 2021. Investigation on CO2-response model of stomatal conductance for plants. Chinese J. Plant Ecol. 45, 420–428. https://doi.org/10.17521/cjpe.2020.0326.

Yu, D., Li, X., Cao, Q., Hao, R., Qiao, J., 2020. Impacts of climate variability and landscape pattern change on evapotranspiration in a grassland landscape mosaic. Hydrol. Process. 34 (4), 1035–1051. https://doi.org/10.1002/hyp.13642.

Zhang, F., Kang, S., Ma, Q., 1999. Effects of CO2 enrichment, nitrogen and water on photosynthesis, evapotranspiration and water use efficiency of spring wheat. J. Basic Sci. Eng. 7, 267–273.

Zhang, Y., Kong, D., Gan, R., Chiew, F.H.S., McVicar, T.R., Zhang, Q., Yang, Y., 2019. Coupled estimation of 500 m and 8-day resolution global evapotranspiration and gross primary production in 2002–2017. Remote Sens. Environ. 222, 165–182. https://doi.org/10.1016/j.rse.2018.12.031.

Zheng, F., Peng, S., 2003. Responses of plant stomatal conductance to elevated CO2 at different scales. Chinese J. Ecol. 22, 26–30.

Zheng, J., Wang, H., Liu, B., 2022. Impact of the long-term precipitation and land use changes on runoff variations in a humid subtropical river basin of China. J. Hydrol. Reg. Stud. 42, 101136.

Zhou, C., Yan, J., Wang, X., Zhou, G., 2005. Long-term comparative study of the hydrological characteristics of forests in different successional stages in the Dinghushan biosphere reserve, Guangdong province. China. Acta Phytoecol. Sin. 29, 208–217.